Resonating-group-method study of $\alpha + {}^{40}$Ca elastic scattering and ^{44}Ti structure

T. Wada
Research Institute for Fundamental Physics, Kyoto University, Kyoto 606, Japan

H. Horiuchi
Department of Physics, Kyoto University, Kyoto 606, Japan

(Received 2 May 1988)

The $\alpha + {}^{40}$Ca elastic scattering cross sections in the energy range from 29.0 to 61.0 MeV are shown to be well reproduced by the resonating-group method by introducing a phenomenological imaginary potential. The local potential equivalent to the nonlocal potential of the resonating-group method is found to be very close to the optical potential of Delbar *et al.* which fits the scattering data well in a wide energy range. Since the optical potential of Delbar *et al.* is the so-called unique optical potential which is free from the discrete ambiguity, this result means that the resonating-group method is powerful and reliable for the study of the internucleus interaction. By calculating the bound and quasibound level spectra by the same $\alpha + {}^{40}$Ca resonating-group method, it is found that the lowest positive parity rotational band is located near the observed ground rotational band of ^{44}Ti. In addition, when we use other effective two-nucleon forces so as to locate the calculated lowest 0^+ state near the observed excited 0^+ state with the excitation energy 8.54 or 11.2 MeV, which has large α strength, the fitting of the elastic scattering data by the resonating-group method is found to be very bad. These results force us to regard that the structure of the ^{44}Ti ground band as containing a large amount of $\alpha + {}^{40}$Ca clustering component. However our present resonating-group method predicts the appearance of the negative parity rotational band with its bandhead 1^- state below the excitation energy 10 MeV although there have been reported no such experimental indications at all of this.

I. INTRODUCTION

In a previous paper[1] the present authors have shown that the calculation by the $\alpha + {}^{16}$O resonating-group method (RGM) with the introduction of a phenomenological imaginary potential reproduces very well not only the spectroscopic data of the bound and quasibound states of ^{20}Ne but also the $\alpha + {}^{16}$O elastic scattering cross section in a wide energy range. Furthermore, they have shown that the equivalent local potential to the RGM nonlocal potential is very similar to the optical potential of Michel *et al.*[2] The optical potential of Ref. 2 is well known as the best α-^{16}O optical potential that fits the scattering cross section in a very wide energy range up to $E_{\rm lab} = 146$ MeV. Since it is now believed that the discrete ambiguity of the optical potentials for light-ion projectiles such as ^{3}He and α is no more existent so long as the high-energy scattering data exhibiting the nuclear rainbow effect is reproduced,[3] the above-mentioned good agreement between the microscopic and optical potentials means the high reliability of the RGM for the study of the internucleus interaction.

In Ref. 1 the effective two-nucleon force is kept fixed in all the energy range up to $E_{\rm lab} = 69.4$ MeV, although at this highest energy a slight modification of the effective two-nucleon force gives a slightly better fitting of the data. A decisive criteria of Ref. 1 for the choice of the effective two-nucleon force was that the spectroscopic data of some low-lying levels of ^{20}Ne including the ground rotational band should be reproduced well by the $\alpha + {}^{16}$O RGM with the adopted two-nucleon force. This was because it is known from the accumulated studies of the ^{20}Ne structure that some characteristic low-lying levels of ^{20}Ne including the ground band should be described well by the microscopic $\alpha + {}^{16}$O cluster model which contains within its model space important SU(3) shell-model configurations.[4] The effective two-nucleon force adopted in Ref. 1 was the Hasegawa-Nagata-Yamamoto (HNY) force.[5] By using this force Matsuse, Kamimura, and Fukushima[6] had already shown that the $\alpha + {}^{16}$O RGM reproduces well the spectroscopic data of the low-lying states of ^{20}Ne.

In order to advance further the RGM study of the internucleus potential, we intended in this paper to make a similar RGM analysis of the $\alpha + {}^{40}$Ca elastic scattering. The reason why we choose the $\alpha + {}^{40}$Ca system for the further RGM study is that like in the $\alpha + {}^{16}$O system there exists also in the $\alpha + {}^{40}$Ca system a very good optical model analysis in a very wide energy range up to $E_{\rm lab} = 166$ MeV which is by Delbar *et al.*[7] In this system it is also regarded that the discrete ambiguity of the optical potential is no more existent.

In making the RGM study, there is an important difference between the $\alpha + {}^{40}$Ca and $\alpha + {}^{16}$O systems. The difference is due to the fact that in the present structure-study of ^{44}Ti it is not so much clarified which levels have large component of the $\alpha + {}^{40}$Ca structure. Therefore, unlike the $\alpha + {}^{16}$O case, it is not easy to use the spectroscopic data of the ^{44}Ti low-lying states in selecting the effective two-nucleon force. One of the present authors

(H.H.) discussed this structure problem in Ref. 8 by comparing two possible standpoints. One is the standpoint that the ground rotational band states should be reproduced approximately as the lowest positive parity rotational band states by the $\alpha+^{40}$Ca RGM calculation. The other is the standpoint that the observed 0^+ state to which the calculated lowest 0^+ state by the $\alpha+^{40}$Ca RGM corresponds is not the ground state but the 8.54 MeV 0^+ state with large α strength.[9] In Ref. 8 two kinds of arguments against the former standpoint were presented and they were regarded to suggest that the latter standpoint is more plausible.

Encouraged by the success of the $\alpha+^{16}$O RGM study in reproducing the data from bound states up to high energy scattering states with a fixed effective two-nucleon force, we proceed in the case of the $\alpha+^{40}$Ca system as follows. Contrary to the $\alpha+^{16}$O study, we first try to fit well the $\alpha+^{40}$Ca elastic scattering cross section in a wide energy range by the RGM with some suitably chosen effective two-nucleon force, and then by using the same two-nucleon force we calculate the bound and quasi-bound states of ^{44}Ti. In this way, we will be able to get very important information to judge which standpoint between the above-mentioned ones is more plausible for the understanding of the ^{44}Ti structure.

We will see in this paper that we can actually fit well the elastic scattering data of $\alpha+^{40}$Ca up to fairly high energy by the RGM with some kind of effective two-nucleon forces. Then we will see that the RGM with such kind of effective two-nucleon forces is favorable for the standpoint that the lowest positive parity rotational band states calculated by the RGM should correspond to the ground rotational band states of ^{44}Ti. This result is contradictory to the two kinds of arguments of Ref. 8, and therefore as we will discuss in this paper we can expect that the resolution of this contradiction will surely advance our understanding of the ^{44}Ti structure. Recently Michel, Reidemeister, and Ohkubo[10,11] have analyzed the fusion excitation function of the $\alpha+^{40}$Ca system by using the optical potential model approach and reached the conclusion that the lowest allowed positive-parity rotational band obtained by the $\alpha+^{40}$Ca local-potential approach should correspond to the ground rotational band of ^{44}Ti. This conclusion is consistent with the conclusion obtained by the present RGM analysis of the scattering data. Hence in the discussion in this paper we will often refer to Refs. 10 and 11.

In this paper, furthermore, we will see that the local potential equivalent to the nonlocal potential of the $\alpha+^{40}$Ca RGM, which fits well the scattering data, is quite close to the optical potential of Delbar *et al.* cited above. This result when combined with the similar success of the $\alpha+^{16}$O RGM (Ref. 1) fortifies our opinion that the RGM is powerful and reliable for the microscopic study of the internucleus interaction including the microscopic foundation of the internucleus optical potential.

This paper is organized as follows. In Sec. II we survey briefly the $\alpha+^{40}$Ca RGM study of the ^{44}Ti structure mainly focusing on what has been the difficulty for the RGM study. In Sec. III we show that by introducing a phenomenological imaginary potential the $\alpha+^{40}$Ca elastic scattering cross section can be reproduced well by the RGM with some kind of effective two-nucleon forces. We see here that the lowest positive parity rotational band calculated by the $\alpha+^{40}$Ca RGM with such kind of two-nucleon forces can be regarded to give an approximate description of the ground rotational band of ^{44}Ti. In Sec. IV we calculate the equivalent local potential to the RGM nonlocal potential which fits well the $\alpha+^{40}$Ca elastic scattering, and then we show that it is quite close to the optical potential by Delbar *et al.* Section V is devoted to discussion and Sec. VI to the conclusion.

II. BRIEF SURVEY OF THE ^{44}Ti STRUCTURE STUDY BY THE $\alpha+^{40}$Ca RGM

In discussing the ^{44}Ti structure by the $\alpha+^{40}$Ca RGM, in Ref. 8, two kinds of the effective two-nucleon forces were compared, namely the Volkov No. 1 force[12] with the Majorana exchange mixture $m=0.623$ and that with $m=0.658$. In both cases the harmonic oscillator parameter ν $(=m\omega/2\hbar)$ was taken to be 0.14 fm^{-2} commonly for α and ^{40}Ca which are both described by the closed-shell configuration of the harmonic oscillator shell model. This value of ν corresponds to $\hbar\omega=11.6$ MeV the value around which is usually adopted as the experimental value of $\hbar\omega$ for ^{40}Ca. The $\alpha+^{40}$Ca RGM with the former choice of m yields its lowest 0^+ state at the observed energy of the ground 0^+ state of ^{44}Ti when the energy is measured from the $\alpha+^{40}$Ca threshold energy. On the other hand, with the latter choice of m the $\alpha+^{40}$Ca RGM yields its lowest 0^+ state at the energy of the observed 0^+ state whose excitation energy is 8.54 MeV. The 8.54 MeV 0^+ state was regarded in Ref. 8 to be lowest among the observed 0^+ states with the large α-spectroscopic strength, except the ground state, according to the experimental study of the reaction ^{40}Ca(^{6}Li,d) of Ref. 9. The comparison of the level spectra by these theoretical calculations with the experiments is displayed again as a part of Fig. 1 in this paper. Like in Refs. 1 and 8, the RGM kernel of the Coulomb interaction (direct plus exchange) is approximated in this paper by $\hat{N}^{1/2}V_{DC}\hat{N}^{1/2}$ where $\hat{N}$ is the RGM norm kernel (direct plus exchange) and V_{DC} is the direct (or double folding) potential of the Coulomb interaction.

In Fig. 1 we see that the theoretical spectrum of the ground band by the Volkov No. 1 force with $m=0.623$ corresponds well to the observed ground state spectrum. This theoretical spectrum is quite similar to that of the $\alpha+^{40}$Ca RGM study[13] by Kihara, Kamimura, and Tohsaki-Suzuki in which it is further reported that the evaluated $E2$ transition rates within the ground band are close to the experimental values. In Fig. 1 we also display the $\alpha+^{40}$Ca RGM level spectra of the ground band by the use of the HNY force[5] with the ^3E strength parameter of the medium range part, $V_m(^3E)=-546+\Delta$ MeV, being given by $\Delta=50$ MeV. In Ref. 1 it is shown that by the use of this HNY force with $\Delta=21.3$ MeV the $\alpha+^{16}$O RGM gives a very good fit to the experimental data from the bound states up to the high energy scattering state. The reason why $\Delta=50$ MeV is chosen here is

explained in the next section where we try to fit the $\alpha+^{40}$Ca scattering data by the RGM.

As is discussed in Ref. 8, although the $\alpha+^{40}$Ca RGM seems to reproduce well the ground band levels of ^{44}Ti, there are strong arguments that this reproduction is not appropriate. One is the problem about the excitation energies of the two theoretical rotational bands, the first negative parity ($K^\pi=0_1^-$) band and the second positive parity ($K^\pi=0_2^+$) band. The $K^\pi=0_1^-$ band is of course calculated to be at the lower excitation energy than the $K^\pi=0_2^+$ band as is seen in Fig. 1. The levels of these two calculated bands have well developed $\alpha+^{40}$Ca dinuclear structure and therefore they should correspond to the observed levels with large α-spectroscopic strength. If we regard that the bandhead 0^+ level of the calculated $K^\pi=0_2^+$ band corresponds to the observed 8.54 MeV 0^+

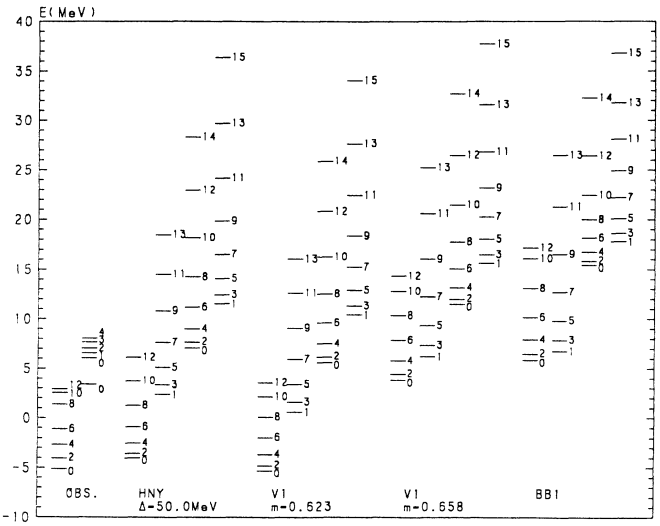

FIG. 1. Experimental and RGM level spectra of ^{44}Ti. In the experimental spectra, only the ground rotational band states and excited states with large α strength are shown. The $\alpha+^{40}$Ca RGM level spectra are shown for four kinds of the effective two-nucleon force, the HNY force with $\Delta=50$ MeV, the Volkov No. 1 force with $m=0.623$, that with $m=0.658$, and the Brink-Boeker force $B1$. The oscillator parameter ν is chosen to be 0.14 fm^{-2} for α and ^{40}Ca which are both described by the closed-shell configuration of the harmonic oscillator shell model and the RGM kernel of the Coulomb interaction (direct plus exchange) is approximated by $\hat{N}^{1/2}\cdot V_{DC}\cdot\hat{N}^{1/2}$ where $\hat{N}$ is the RGM norm kernel (direct and exchange) and V_{DC} is the direct (or double folding) potential of the Coulomb interaction. The unbound states are treated within the bound state approximation. Energies are measured from the $\alpha+^{40}$Ca threshold energy. All the levels have the natural parity and so the parity designation is omitted. The level spectra by use of the Brink-Boeker $B1$ force are slightly different from those reported in Refs. 18 and 19. This may be due to the difference between ours and Refs. 18 and 19 of the approximate calculation of Coulomb kernel and of the energy calculation of the quasibound states which is done in Refs. 18 and 19 without using the bound state approximation.

level, we encounter a serious difficulty that, in the energy region lower than the 8.54 MeV 0^+ level, we have no observed negative parity rotational band which should correspond to the calculated $K^\pi=0_1^-$ band. In other words, as is seen in Fig. 1, the calculated energy gap between the bandhead state of the lowest $K^\pi=0^+$ band and that of the lowest $K^\pi=0^-$ band is found to be smaller than about 7 MeV, but until now we have no experimental report on the existence of the $K^\pi=0^-$ band below the excitation energy 10 MeV. According to the ^{40}Ca(α,α) experiment of Refs. 14 and 15, aside from the 8.54 MeV 0^+ state and the ground band states, the observed states with large α strength are a group of states with $J^\pi=0^+$, 1^-, 2^+, and 3^- with the excitation energy (E_x), 11.2, 11.7, 12.2, and 12.8 MeV, respectively. Thus as explained in Ref. 8, in our present experimental knowledge the lowest observed 1^- state with large α strength is located at 11.7 MeV. It is very inappropriate to assign the bandhead 1^- state of the calculated $K^\pi=0_1^-$ band to this observed 11.7 MeV 1^- state because the difference of the excitation energies between the theoretical and experimental 1^- states is too large. It is to be mentioned that this problem about the location of the $K^\pi=0_1^-$ and 0_2^+ bands was also regarded to be a serious question on the structure of ^{44}Ti in the report[16] by Arima who discussed the α-clustering problem of ^{44}Ti on the basis of the work with Tomoda in which the $\alpha+^{40}$Ca RGM was extended so as to include into its model space all the $0f1p$ shell-model states with [4] and [31] spatial symmetries.

Another argument against the assignment of the RGM lowest 0^+ state to the ^{44}Ti ground state is due to the recognition of the strong effect of the spin-orbit force in the ground band states. When the configurations, especially with the broken spatial symmetries, are introduced into the model space in addition to the [4] symmetry states of the $\alpha+^{40}$Ca RGM, the calculated structure of the ground rotational band may be no more dominated by the $\alpha+^{40}$Ca structure by the effect of the spin-orbit force. Such kinds of theoretical studies were actually performed by Itonaga[17] and by Tomoda and Arima.[16] Itonaga concluded that the $\alpha+^{40}$Ca clustering component is very small while in Ref. 16 the $\alpha+^{40}$Ca component was calculated to be 60–70 % in its squared amplitude. Moreover, Arima suggested that the inclusion of the broken symmetries [22], [211], and [1111] which were missing in Ref. 16 might push the ground band wave functions further toward the $(0f_{7/2})^4$ configurations allowing the appearance of states within the $\alpha+^{40}$Ca functional space not in the ground band but in some excited band.

The above-mentioned two arguments were regarded in Ref. 8 to suggest that the observed 0^+ state to which the calculated lowest 0^+ state by the $\alpha+^{40}$Ca RGM corresponds is not the ground state but the 0^+ state at 8.54 MeV. As we see in Fig. 1, if we adopt the Volkov No. 1 force with $m=0.658$, so as to reproduce the RGM lowest 0^+ state at the position of the 8.54 MeV 0^+ state, the observed 1^- state at 11.7 MeV seems to be well reproduced by the bandhead 1^- state of the theoretical lowest $K^\pi=0^-$ band. Friedrich and Langanke[18,19] made $\alpha+^{40}$Ca RGM studies by using the same ν as ours and

the Brink-Boeker force $B1$ (Ref. 20) as the effective two-nucleon interaction, and they obtained as the lowest rotational band a parity-mixed rotational band[21] ($J^\pi=0^+,1^-,2^+,3^-,\ldots$) starting with the 0^+ state at 5.1 MeV above the $\alpha+^{40}$Ca threshold. This calculated band was regarded[19,15] to correspond well to a group of observed states with $J^\pi=0^+$, 1^-, 2^+, and 3^- (with $E_x=11.2$, 11.7, 12.2, and 12.8 MeV, respectively) which were interpreted experimentally in Ref. 15 also as members of a mixed-parity rotational band. The $\alpha+^{40}$Ca RGM level spectra by the use of the Brink-Boeker $B1$ force are also displayed in Fig. 1.

In the next section we calculate the $\alpha+^{40}$Ca elastic scattering angular distribution by the RGM by using

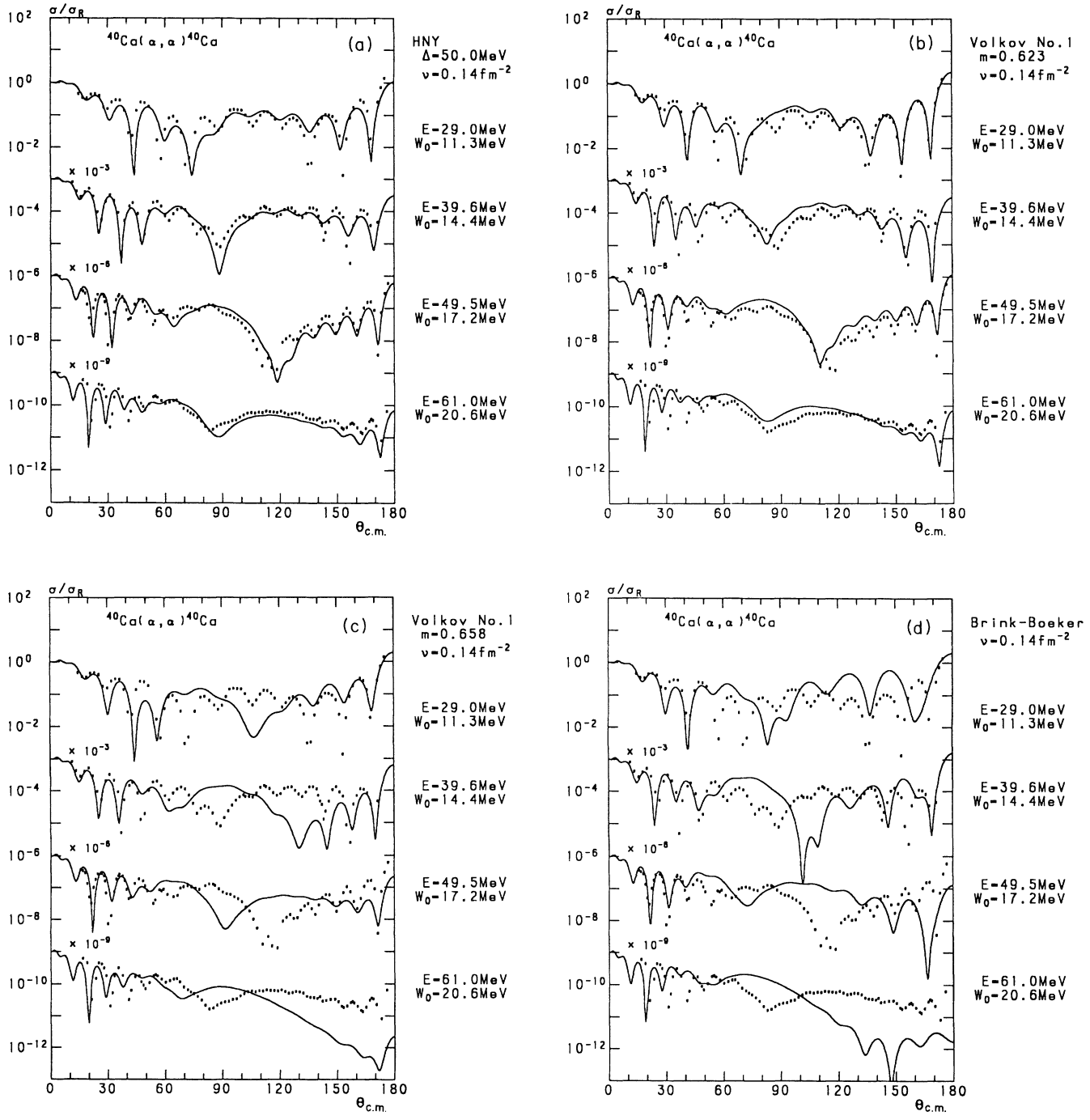

FIG. 2. Comparison of the experimental data (dots) for $\alpha+^{40}$Ca elastic scattering with the calculations (solid curves) by the $\alpha+^{40}$Ca RGM with four kinds of effective two-nucleon force; the HNY force with $\Delta=50$ MeV (a), the Volkov No. 1 force with $m=0.623$ (b), the Volkov No. 1 force with $m=0.658$ (c), and the Brink-Boeker force $B1$ (d). The experimental data are due to Refs. 7 and 47–50.

above-mentioned four kinds of the effective two-nucleon force, the HNY force with $\Delta=50$ MeV, the Volkov No. 1 force with $m=0.623$, that with $m=0.658$, and the Brink-Boeker force $B1$. As seen in Fig. 1, use of the former two kinds of nuclear force corresponds to the standpoint that the ground rotational band should be reproduced approximately as the lowest rotational band by the $\alpha+^{40}$Ca RGM, while use of the latter two corresponds to the standpoint that the observed 0^+ state which is to be described by the lowest 0^+ state by the $\alpha+^{40}$Ca RGM is not the ground state but some excited 0^+ state with large α strength, either the 8.54 MeV 0^+ state or 11.2 MeV 0^+ state. Encouraged by the success[1] of the $\alpha+^{16}$O RGM in reproducing the data from bound states up to high energy scattering states, we expect that the $\alpha+^{40}$Ca RGM will succeed in reproducing the experimental angular distribution up to high scattering energy by using the effective two-nucleon force based on one of the above-mentioned two standpoints. This means that we expect the scattering data will give us powerful new information to judge which standpoint is more plausible.

III. ANALYSIS OF THE $\alpha+^{40}$Ca ELASTIC SCATTERING CROSS SECTION BY THE RGM

By using four kinds of effective two-nucleon force which are explained in Sec. II and with which the bound and quasibound level spectra are calculated as shown in Fig. 1, we have calculated the $\alpha+^{40}$Ca elastic scattering cross sections by the RGM under the introduction of a phenomenological imaginary potential into the RGM equation of motion as follows:

$$[\hat{H}+\sqrt{\hat{N}}iW(r)\sqrt{\hat{N}}-E_r\hat{N}]\chi=0\ , \tag{3.1}$$

where $\hat{H}$ and $\hat{N}$ are the Hamiltonian and norm RGM kernels,[22,23] respectively. The choice of the oscillator parameter and the construction of the Coulomb kernel in $\hat{H}$ are made in the same way as in the calculation of the level spectra displayed in Fig. 1. Here E_r is the scattering energy in the center-of-mass frame and $W(r)$ is of the squared Woods-Saxon form

$$W(r)=-W_0(E)\{1+\exp[(r-R_I)/a_I]\}^{-2}\ . \tag{3.2}$$

In view of the excellent reproduction of the experimental scattering cross section by the optical potential of Ref. 7, the values of $W_0(E)$, R_I, and a_I have been chosen to be the same as those of Ref. 7; namely

$$W_0(E)=2.99+0.288E \text{ MeV}\ ,$$
$$R_I=6.0 \text{ fm},\quad a_I=1.0 \text{ fm}\ . \tag{3.3}$$

Here E stands for the α-particle energy in the laboratory frame.

The comparison of the angular distributions between the RGM calculations and the data is shown in Fig. 2 for $E=29.0$, 39.6, 49.5, and 61.0 MeV, and for the adopted four kinds of effective nuclear force. We can see that the data fitting in (a) and (b) of Fig. 2 is fairly good while that in (c) and (d) of Fig. 2 is band. The large disagreement of the dip positions between theory and experiment in the intermediate angle region ($60°<\theta<120°$) of (c) and (d) of Fig. 2 has not been able to be diminished by changing the parameter values of the imaginary potential $W(r)$ from those of Eq. (3.3).

The good data fitting in (a) and (b) of Fig. 2 leads to the following two conclusions: Firstly, in addition to the $\alpha+^{16}$O system,[1] also in the $\alpha+^{40}$Ca system, the RGM

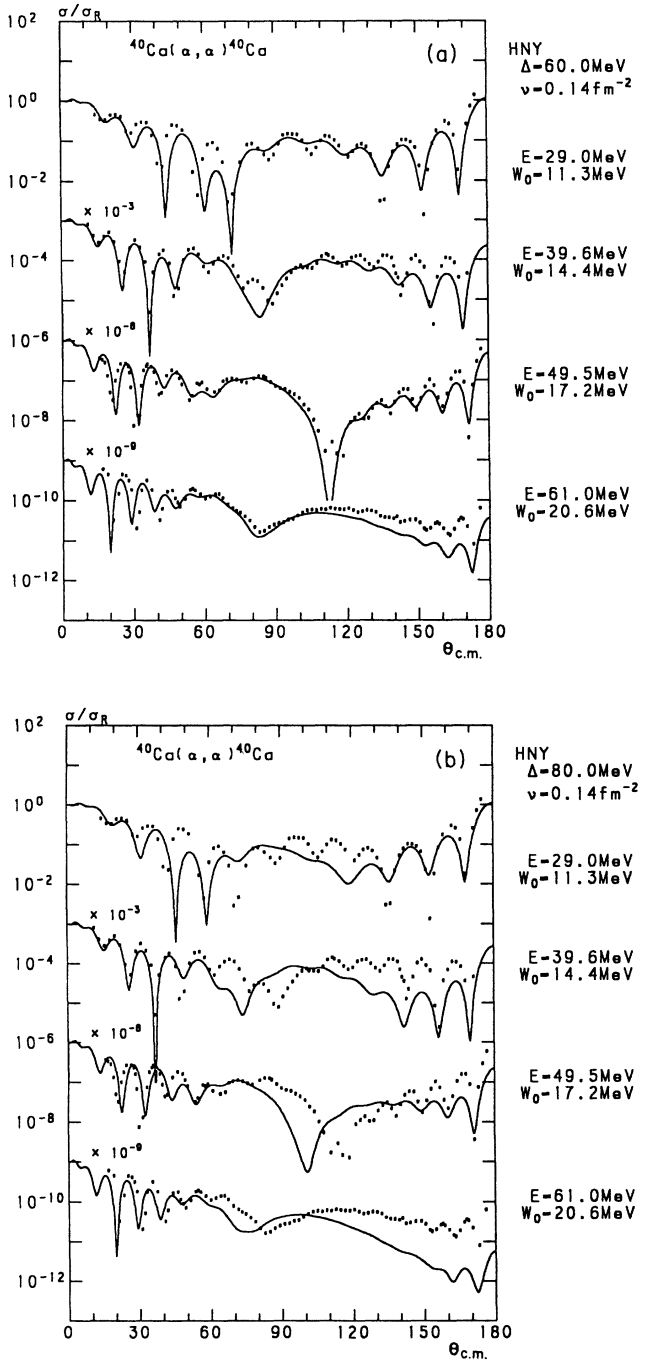

FIG. 3. Similar comparison as in Fig. 2 of the $\alpha+^{40}$Ca elastic scattering data (dots) with the $\alpha+^{40}$Ca RGM calculations (solid curves) with the HNY force. (a) is for $\Delta=60$ MeV and (b) is for $\Delta=80$ MeV.

with fixed effective two-nucleon force has proved to give a good fit to the scattering data in a wide energy range. This fortifies our opinion that the RGM is reliable for the microscopic study of the internucleus interaction process. Secondly, when combined with the result that the data fitting in (c) and (d) of Fig. 2 is bad, we are forced to support the standpoint that the lowest rotational band by the $\alpha+^{40}$Ca RGM should be regarded to give us an approximate description of the ground rotational band of ^{44}Ti.

In order to see in a more quantitative way how restrictive the condition is which the scattering data fitting imposes on the selection of the effective two-nucleon force, we study the change of the scattering data fitting and of the bound and quasibound level spectra against the change of the Δ parameter of the HNY force adopted for the $\alpha+^{40}$Ca RGM. In Fig. 3, the RGM angular distributions by the HNY force with $\Delta=60$ MeV and with $\Delta=80$ MeV are compared with experiments. We see that the data fitting by $\Delta=60$ MeV is of similar quality as that by $\Delta=50$ MeV displayed in Fig. 2(a), while that by $\Delta=80$ MeV is bad like in (c) and (d) of Fig. 2. From the comparison of the data fittings by $\Delta=50$, 60, and 80 MeV, we may conclude that the allowable range of the value of the Δ parameter of the HNY force is 50 MeV $\lesssim\Delta\lesssim$ 60 MeV. In Fig. 4 we show the change of the bound and quasibound level spectra of the RGM against the change of the Δ parameter of the HNY force adopted for the RGM. We see that by changing the Δ value from 50 to 60 MeV, the binding energy of the lowest 0^+ state becomes smaller by a rather large amount, about 3 MeV, while the energy of the second 0^+ changes by only 0.8 MeV. Thus if the HNY force with $\Delta=60$ MeV proves to be a suitable effective force to be adopted for the $\alpha+^{40}$Ca RGM, it will be necessary for the ground-state wave function of ^{44}Ti to have rather large amount of other configurations than the antisymmetrized $\alpha+^{40}$Ca configuration in order to reproduce the observed binding energy.

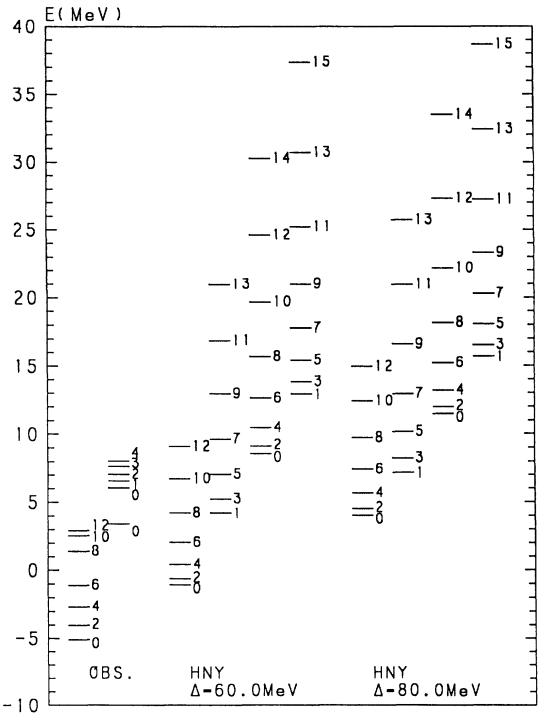

FIG. 4. ^{44}Ti level spectra calculated by the $\alpha+^{40}$Ca RGM by the use of the HNY force with $\Delta=60$ MeV and $\Delta=80$ MeV. The experimental spectrum is also shown for the sake of comparison.

It is quite important that the result of the RGM analysis of the scattering data in a wide energy range is favorable for the standpoint that the lowest rotational band by the RGM gives an approximate description of the observed ground band, and therefore we will discuss what this means in Sec. V.

It is to be noted that the good data fitting in (a) and (b) of Fig. 2 is obtained by the use of the imaginary potential of Ref. 7 without any modification [Eqs. (3.2) and (3.3)], and by using the effective two-nucleon force independent of the scattering energy. An even better fit to the data will be obtained in the present RGM framework by modifying the parameters of the imaginary potential and by changing the parameters of the effective two-nucleon force for different energies E as was discussed in Ref. 1.

IV. COMPARISON OF THE EQUIVALENT LOCAL POTENTIAL WITH THE OPTICAL POTENTIAL

As seen in Sec. III we can fit well the elastic scattering data of $\alpha+^{40}$Ca up to fairly high energy by the RGM with some kind of effective two-nucleon forces. We, therefore, construct the equivalent local potential (ELP) from this RGM nonlocal interaction by the method of Ref. 24, and compare it with the optical potential $V^{\rm opt}(r)$ of Ref. 7. The imaginary part of this $V^{\rm opt}(r)$ is given by Eqs. (3.2) and (3.3) and the real part of its is expressed as

$$V(r)=-V_0(E)\{1+\exp[(r-R)/a]\}^{-2}\ ,$$
$$V_0(E)=198.6\times(1-0.00168E)\ \text{MeV}\ , \qquad (4.1)$$
$$R=4.68\ \text{fm},\quad a=1.29\ \text{fm}\ .$$

As the RGM nonlocal interaction to be analyzed, we adopt the one constructed by the use of the HNY force with $\Delta=50$ MeV. The ELP, $V_l^{\rm ELP}(r)$ depends slightly on the angular momentum l of the relative motion, and hence in order to compare the ELP with the angular-momentum-independent optical potential, we use the l-averaged ELP, $V^{\rm ELP}(r)$, defined as follows:

$$V^{\rm ELP}(r)=\sum_l I_l V_l^{\rm ELP}(r)\Big/\sum_l I_l\ ,$$
$$I_l=(2l+1)\,|\,1-\exp(2i\delta_l)\,|^{\,2}\ , \qquad (4.2)$$

where δ_l denotes the nuclear phase shift. This l-averaged ELP was used also in Ref. 1. Figure 5 displays the comparison of the shape of $V^{\rm ELP}(r)$ with that of $V^{\rm opt}(r)$ at $E=29.0$ and 61.0 MeV. We see that $V^{\rm ELP}(r)$ is quite close to $V^{\rm opt}(r)$. Together with the similar result in the $\alpha+^{16}$O system,[1] we can say that the RGM is powerful and reliable for the study of the microscopic foundation

of the internucleus optical potential.

We next study the volume integral per nucleon pair, j_V, of the real part of $V^{\rm ELP}(r)$; $j_V=\int dr\,{\rm Re}[V^{\rm ELP}(r)]/160$. Figure 6 shows by dot points j_V of ${\rm Re}[V^{\rm ELP}(r)]$ at $E=29.0$, 39.6, 49.5, and 61.0 MeV. For the sake of comparison we also display j_V of ${\rm Re}[V_l^{\rm ELP}(r)]$ with $l=0$. It is to be noticed that the l-average procedure reduces the value of j_V of ${\rm Re}[V_l^{\rm ELP}(r)]$ with $l=0$ by about 20–25 MeV fm^3 in the energy region treated in this paper. The value of j_V for the real part of $V^{\rm opt}(r)$ of Ref. 7 is given by the straight dotted line. At $E=29.0$ MeV the difference of j_V between ${\rm Re}[V^{\rm ELP}(r)]$ and ${\rm Re}[V^{\rm opt}(r)]$ looks rather large. This difference is due to the rather large difference of ${\rm Re}[V^{\rm ELP}(r)]$ from ${\rm Re}[V^{\rm opt}(r)]$ in the tail region as is seen in Fig. 5(a). Here we should be reminded that j_V of ${\rm Re}[V^{\rm opt}(r)]$ of Ref. 7 in the energy region $E\lesssim 30$ MeV is larger than j_V of ${\rm Re}[V^{\rm opt}(r)]$ obtained by the model-independent optical model analyses by Michel and Vanderpoorten[25] and by Gubler *et al.*[26] Following Refs. 25 and 26, Michel *et al.*[10] modified the depth parameter $V_0(E)$ of Eq. (4.1) to the fixed value, 180 MeV, in the energy range 10 MeV $\lesssim E\lesssim$ 30 MeV, which results in the value of j_V of ${\rm Re}[V^{\rm opt}(r)]$, 350 MeV fm^3.

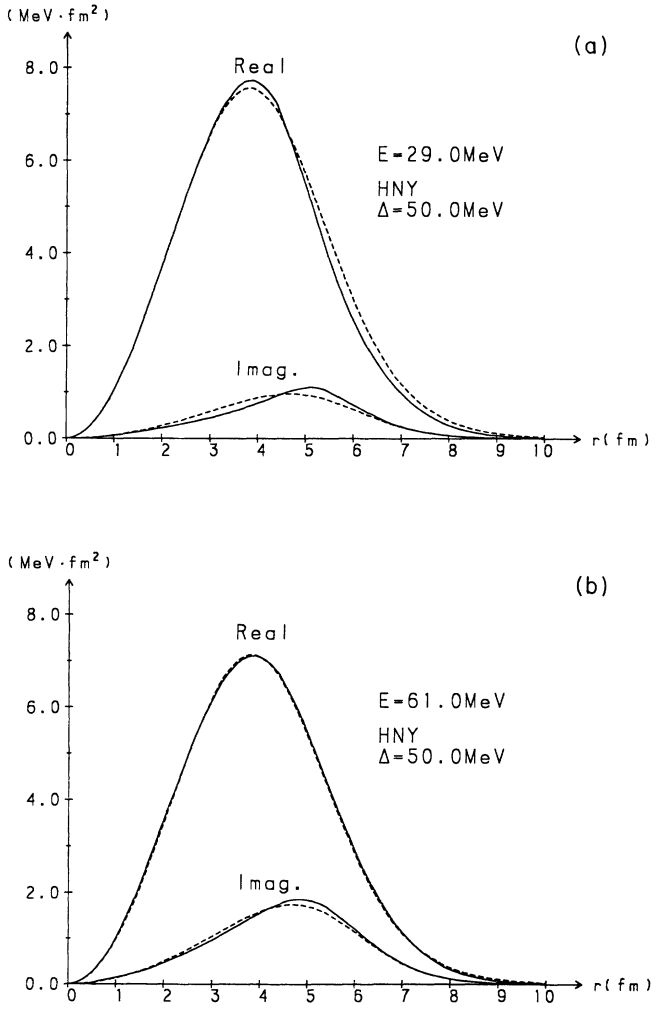

FIG. 5. Comparison of the shape of $r^2V^{\rm opt}(r)/160$ (dashed curve) with that of $r^2V^{\rm ELP}(r)/160$ (solid curve) calculated by the use of the HNY force with $\Delta=50$ MeV. (a) is for $E=29.0$ MeV and (b) is for $E=61.0$ MeV.

It is instructive to analyze the difference of j_V between ${\rm Re}[V^{\rm ELP}(r)]$ and ${\rm Re}[V_l^{\rm ELP}(r)]$ with $l=0$. As is clarified in previous studies,[27,28] in general, $V_l^{\rm ELP}(r)$ becomes shallower quite slowly as l increases. Thus, in general, the l-averaged ELP, $V^{\rm ELP}(r)$ is shallower than $V_l^{\rm ELP}(r)$ with $l=0$. In order to understand the effect of the l-average procedure, the present authors proposed in Ref. 28 to compare $V^{\rm ELP}(r)$ with $V_{l_g}^{\rm ELP}(r)$ where l_g is the effective grazing angular momentum defined by

$$l_g=kR=\left[\frac{2\mu}{\hbar^2}E\right]^{1/2}R\ . \tag{4.3}$$

In Fig. 6 there are also shown by solid curves j_V of ${\rm Re}[V_{l_g}^{\rm ELP}(r)]$ with l_g for $R=3.9$, 4.5, and 5.2 fm. We see that in the energy range (30 MeV $\lesssim E\lesssim$ 60 MeV) treated in this paper j_V of ${\rm Re}[V^{\rm ELP}(r)]$ is simulated rather well by j_V of ${\rm Re}[V_{l_g}^{\rm ELP}(r)]$ with l_g for $R=4.5$ fm.

In Sec. III we have seen that the quality of the scattering data fitting by the use of the HNY force with $\Delta=60$ MeV is almost the same as that with $\Delta=50$ MeV. Therefore, in the final part of this section we make the comparison of the optical potential $V^{\rm opt}(r)$ of Ref. 7 with the ELP constructed by the use of the HNY force with $\Delta=60$ MeV. Figure 7 displays the similar comparison as Fig. 5 between the shape of $V^{\rm opt}(r)$ and that of the l-averaged ELP $V^{\rm ELP}(r)$ by this effective force at $E=29.0$ and 61.0 MeV. We see that here also $V^{\rm ELP}(r)$ is quite close to $V^{\rm opt}(r)$.

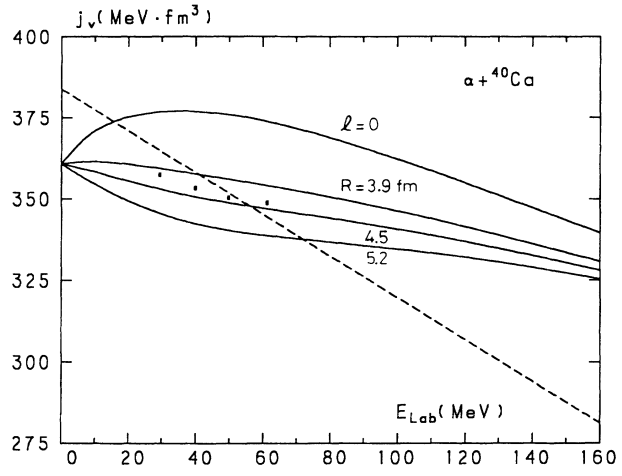

FIG. 6. Comparison of the volume integral per nucleon pair, j_V, of the real part of the optical potential (straight dashed line, Ref. 7) with that of the l-averaged equivalent local potential $V^{\rm ELP}(r)$ of Eq. (4.2) (dots). The solid curved indicated as $l=0$ shows j_V of ${\rm Re}[V_l^{\rm ELP}(r)]$ with $l=0$. Here are also shown j_V of ${\rm Re}[V_{l_g}^{\rm ELP}(r)]$ with l_g defined by Eq. (4.3) for three values of R in terms of the solid curves indicated by the respective values of R.

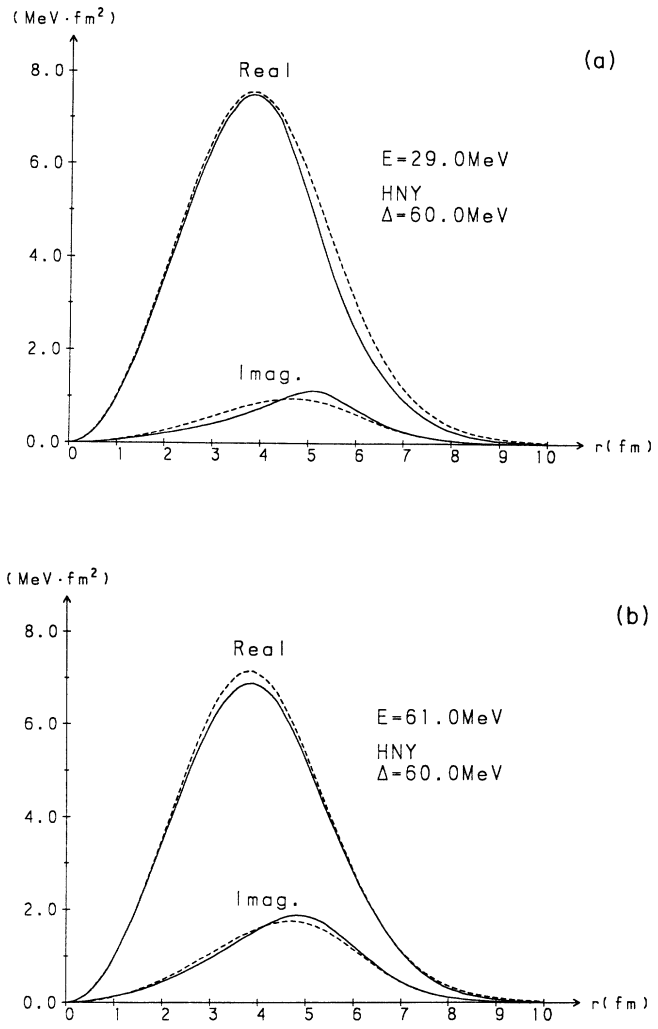

FIG. 7. The same comparison as Fig. 5 by the use of the HNY force with $\Delta = 60$ MeV.

V. DISCUSSION

In Sec. III we have seen that the $\alpha + {}^{40}$Ca elastic scattering cross section can be fitted well by the $\alpha + {}^{40}$Ca RGM if the effective two-nucleon force is suitably chosen. The HNY force with 50 MeV $\lesssim \Delta \lesssim$ 60 MeV and the Volkov No. 1 force with $m = 0.623$ are such kind of suitable effective two-nucleon force. An important characteristic property of such kind of suitable effective two-nucleon force is that the calculated lowest 0^+ state is located below the $\alpha + {}^{40}$Ca threshold and the calculated second 0^+ state is located at about 6.5 MeV above the $\alpha + {}^{40}$Ca threshold. On the other hand, we have also seen that if we use the effective two-nucleon force that locates the calculated lowest 0^+ state at the position of the observed 8.54 MeV 0^+ state (3.4 MeV above the $\alpha + {}^{40}$Ca threshold) or the observed 11.2 MeV 0^+ state (6.06 MeV above the threshold), the fitting of the calculated cross section to the experimental one is very bad.

Based on these two results we have concluded in Sec. III that the analysis of the $\alpha + {}^{40}$Ca scattering data by the RGM forces us to support the standpoint that the lowest rotational band by the $\alpha + {}^{40}$Ca RGM should be regarded to give us an approximate description of the ground rotational band of ^{44}Ti. This result of Sec. III is consistent with the conclusion of the recent study of the $\alpha + {}^{40}$Ca fusion cross section of Refs. 10 and 11 by the optical potential model approach which was based on the recipe used extensively by Hatogai, Ohta, and Okai.[29] In Ref. 10, the $\alpha + {}^{40}$Ca optical potential of Ref. 7 was adopted with minor modifications of the strength parameters of its real and imaginary parts, and the fusion cross sections were regarded to be obtained by the reaction cross section calculated by reducing the imaginary potential radius. After ascertaining the good theoretical reproduction of the oscillatory fusion cross section in the region of $E = 10$–27 MeV, the authors of Ref. 10 calculated bound and quasibound level spectra by using the real part of the adopted optical potential. They found that the lowest rotational band allowed by the Pauli principle appears in the energy region quite close to the observed ground band. Thus they insisted[10,11] that the ground band structure can be approximated well by the $\alpha + {}^{40}$Ca cluster structure.

It is to be noticed that the approach of Refs. 10 and 11 which uses the phenomenological local potential is not free from some ambiguities in making quantitative agreements. For example, as is shown in Ref. 30 by the same authors, the use of the optical potential of Ref. 26, which also fits the scattering data very well, locates the lowest Pauli-allowed 0^+ level at about 6 to 9 MeV below the $\alpha + {}^{40}$Ca threshold, while in Refs. 10 and 11 it is located at 3.67 MeV below the threshold. In Refs. 10 and 11, the wave functions of bound and quasibound states are calculated by the use of the real part of the optical potential for $E = 10$–30 MeV. From the viewpoint of the microscopic theory, however, this recipe may not be so reliable quantitatively. This is because according to the study of the energy dependence[27,28,31–35] of the equivalent local potential to the RGM nonlocal potential, the change of the potential shape, especially in its tail region, is rapid when the scattering energy goes down to zero in the low-energy region. Namely the microscopic potential becomes more attractive in the inner spatial region and more repulsive rapidly in the tail region as the energy goes down. And, furthermore, according to our preliminary investigation this tendency of the energy dependence continues to be the same as the relative-motion energy goes down in the negative energy region. In this respect, it is instructive that the effective $\alpha + {}^{16}$O potentials for the ground band levels constructed in Ref. 6 from the $\alpha + {}^{16}$O RGM nonlocal potentials and also the effective $\alpha + {}^{40}$Ca potentials for the lowest rotational band levels constructed in Ref. 13 from the $\alpha + {}^{40}$Ca RGM nonlocal potentials, are even repulsive in the tail region with their repulsive height reaching to about 5 MeV for the former and to about 10 MeV for the latter. These

kinds of potentials are, of course, unable usually to be obtained from the real part of the optical potential.

According to Sec. III the location of the lowest 0^+ state by the $\alpha+^{40}$Ca RGM is determined with an ambiguity of about 5 MeV. If we follow the conjecture by Arima in Ref. 16, in order to construct the ground-state wave function of ^{44}Ti, we need to mix other components than the $\alpha+^{40}$Ca one more than 40% in their total squared amplitudes. The location of the lowest 0^+ state by the $\alpha+^{40}$Ca RGM is strongly correlated with the magnitude of the amplitudes of the above-mentioned mixing components in obtaining the good wave function for the ground state of ^{44}Ti.

The most serious objection to the result of Sec. III is just the argument emphasized in Ref. 8 and explained again in Sec. II. Namely, if the lowest 0^+ state by the $\alpha+^{40}$Ca RGM should appear in the energy region close to the observed ground state of ^{44}Ti, the appearance of the negative parity rotational band with its band head 1^- state below 10 MeV cannot be avoided in spite of the fact that there have been reported no such experimental indications at all. This difficulty was already noticed in Ref. 13 and was regarded in Ref. 16 to be a serious question on the structure of ^{44}Ti. This difficulty is equally existent in the result of the above-cited works of Refs. 10 and 11. The authors of Refs. 10 and 11 have discussed this problem seriously and have insisted that there should exist a $K^\pi=0^-$ rotational band starting just above the threshold which should be, therefore, actively searched for experimentally. The answer of the present authors to this problem is the same as that of Ref. 10 and 11 mentioned above because the result of the analyses of Sec. III inevitably leads to this answer. As for the quantitative prediction of the location of the bandhead 1^- level, the analyses of Sec. III suggest that the 1^- energy is located in the region from 0 to 5 MeV above the threshold.

In order to show the outline of the wave functions of the lowest rotational band levels obtained by the $\alpha+^{40}$Ca RGM, we give in Table I the calculated values of the rms intercluster distance $\langle R^2\rangle^{1/2}$ and intraband $B(E2)$. The value $\langle R^2\rangle^{1/2}$ is obtained first by calculating the ordinary rms radius $\langle r^2\rangle_{\rm Ti}^{1/2}$ by the RGM wave function and next by using the following equation:

$$44\langle r^2\rangle_{\rm Ti}=4\langle r^2\rangle_\alpha+40\langle r^2\rangle_{\rm Ca}+\frac{4\times 40}{44}\langle R^2\rangle\ , \quad (5.1)$$

where $\langle r^2\rangle_\alpha^{1/2}$ and $\langle r^2\rangle_{\rm Ca}^{1/2}$ are the rms radius of α and ^{40}Ca, respectively, and are calculated by the harmonic oscillator closed-shell wave functions with the common oscillator parameter ν used for the $\alpha+^{40}$Ca RGM. The effective two-nucleon forces used in the RGM calculation are the HNY force with $\Delta=50$ and 60 MeV. In Table I the experimental $B(E2)$ values of the ground band are shown compared with the calculated values. We see that the calculated $B(E2)$ values are large and rather close to the observed values especially in the case of $\Delta=60$ MeV. It is to be noticed here that no effective charge is used in the calculation while in $(fp)^4$ shell-model calculations one needs large effective charge ($\delta e\sim 0.5e$) in order to reproduce the observed values.[17]

The calculated rms intercluster distance is seen to decrease as the spin of the state increases from 0 to 12. This antistretching effect[36] is well known to exist in the ground band of ^{20}Ne.[4] This effect means that the degree of clustering becomes weaker when going from the 0^+ to the 12^+ state. In Table I we have shown the squared amplitude of the SU(3) shell model component $(pf)^4$[4](12,0) contained in the RGM wave function for each spin state. These amplitudes clearly show that the RGM wave function approaches more and more to the SU(3) shell-model limit as the spin of state increases. Now as for the comparison with experiments, the observed rms charge radius of the ^{44}Ti ground state which is 3.60 fm (Ref. 37) is the only quantity to be compared with the calculation. The calculated rms charge radius which is equivalent to $\langle r^2\rangle_{\rm Ti}^{1/2}$ in the present model is 3.37 fm or $\Delta=50$ MeV and 3.39 fm for $\Delta=60$ MeV in the case of the lowest 0^+ state.

Here we should point out that a careful treatment of the antisymmetrization effect is necessary when one calculates the quantities like $B(E2)$ values and rms radii by using the wave functions which describe the states with strong overlap between clusters. As we show below, the calculated $B(E2)$ values of Ref. 11 (and 30) and of Ref. 13 are overestimated by about 15–30 % compared with the values by the proper treatment. First consider the calcu-

TABLE I. Values of the rms intercluster, distance, intraband $B(E2)$, and the squared amplitude α^2 of the SU(3) shell-model component $(pf)^4$[4](12,0), for the states of the calculated lowest rotational band. Theoretical values are obtained for two kinds of the HNY force, one with $\Delta=50$ MeV and the other with $\Delta=60$ MeV. As for the $B(E2)$ values, the experimental ones of the ground rotational band (Ref. 51) are also shown for the sake of the comparison. Here J stands for the total angular momentum and is of course equal to the relative angular momentum l between α and ^{40}Ca.

	$\langle R^2\rangle^{1/2}$ (fm)		$B(E2)(J\to J-2)(e^2\text{fm}^4)$			α^2	
J^π	$\Delta=50$	$\Delta=60$	$\Delta=50$	$\Delta=60$	Exp.	$\Delta=50$	$\Delta=60$
0^+	4.09	4.25				0.87	0.80
2^+	4.07	4.21	72.2	83.5	120±30	0.88	0.81
4^+	4.01	4.14	95.2	109.2	280±60	0.90	0.84
6^+	3.94	4.04	90.3	102.4	160±20	0.92	0.88
8^+	3.86	3.93	74.7	83.5	>14	0.95	0.91
10^+	3.77	3.82	53.0	58.2	140±30	0.97	0.95
12^+	3.69	3.71	27.3	29.5	40±8	0.99	0.98

lation by the local potential model of Ref. 11 (and 30). In this model the $B(E2)$ matrix element is simply given by

$$M_l' = \langle u_{l-2}(r)Y_{l-2,0}(\hat{r}) \mid \tilde{y}_{20}(\mathbf{r}) \mid u_l(r)Y_{l0}(\hat{r}) \rangle \ , \qquad \tilde{y}_{20}(\mathbf{r}) = \frac{4\times 40}{44} y_{20}(\mathbf{r}), \quad y_{20}(\mathbf{r}) = r^2 Y_{20}(\hat{r}) \ , \tag{5.2}$$

where $u_l(r)$ is the eigenstate wave function with the angular momentum l for a given local potential. As is supposed in Ref. 30, it is usual[38-40] to link $u_l(r)Y_{l0}(\hat{r})$ to the RGM wave function,

$$\Phi_l = \begin{bmatrix} 44 \\ 4 \end{bmatrix}^{-1/2} \mathcal{A}[(\hat{N}^{-1/2} u_l(r)Y_{l0}(\hat{r}))\phi(\alpha)\phi(^{40}\mathrm{Ca})] \ , \tag{5.3}$$

where $\phi(\alpha)$ and $\phi(^{40}\mathrm{Ca})$ stand for the internal wave functions of α and ^{40}Ca, respectively, $\mathcal{A}$ is the antisymmetrizing operator and $\hat{N}$ the RGM norm kernel. According to this link, the $B(E2)$ matrix element by the proper treatment of the antisymmetrization effect is given as follows:

$$M_l = \langle \Phi_{l-2} \mid \sum_{i=1}^{44} y_{20}(\mathbf{r}_i - \mathbf{X}_G) \mid \Phi_l \rangle \ , \tag{5.4}$$

where $\mathbf{X}_G$ stands for the total center-of-mass coordinate. In our present treatment where $\phi(\alpha)$ and $\phi(^{40}\mathrm{Ca})$ are expressed by the harmonic oscillator (HO) shell-model wave functions with common oscillator parameter ν, the eigenfunctions of the norm kernel $\hat{N}$ are HO wave functions $u_{Nl}^{\mathrm{HO}}(r)Y_{lm}(\hat{r})$ with oscillator parameter $\gamma = \mu\nu$, where μ is the reduced mass number ($\mu = \frac{40}{11}$) and N the number of the oscillator quanta, $N = 2n + l$ with n standing for the number of radial nodes. The eigenfunction expansion of $\hat{N}$ is expressed by

$$\hat{N} = \sum_N \mu_N \sum_{lm} \mid u_{Nl}^{\mathrm{HO}}(r)Y_{lm}(\hat{r}) \rangle \langle u_{Nl}^{\mathrm{HO}}(r)Y_{lm}(\hat{r}) \mid \ , \tag{5.5}$$

which is because the eigenvalues μ_N depend only on N and not on l.[23,41] By using Eq. (5.5) and the expansion of $u_l(r)$ by $u_{Nl}^{\mathrm{HO}}(r)$,

$$u_l(r) = \sum_N C_{Nl} u_{Nl}^{\mathrm{HO}}(r) \ , \tag{5.6}$$

we can express the matrix elements M_l' and M_l as follows:[23]

$$\begin{aligned} M_l' &= \sum_{N,N'} C_{Nl-2} C_{N'l} m(N,N',l) \ , \\ M_l &= \left[\sum_{N \le N'} \left[\frac{\mu_N}{\mu_{N'}} \right]^{1/2} + \sum_{N > N'} \left[\frac{\mu_{N'}}{\mu_N} \right]^{1/2} \right] C_{Nl-2} C_{N'l} m(N,N',l) \ , \\ m(N,N',l) &= \langle u_{Nl-2}^{\mathrm{HO}}(r)Y_{l-2,0}(\hat{r}) \mid \tilde{y}_{20}(\mathbf{r}) \mid u_{N'l}^{\mathrm{HO}}(r)Y_{l0}(\hat{r}) \rangle \\ &= \langle u_{Nl-2}^{\mathrm{HO}} \mid r^2 \mid u_{N'l}^{\mathrm{HO}} \rangle \cdot \frac{4\times 40}{44} \langle Y_{l-2,0} \mid Y_{20} \mid Y_{l0} \rangle \ . \end{aligned} \tag{5.7}$$

In the present $\alpha + ^{40}$Ca RGM, μ_N for $N < 12$ are zero, which means that $u_{Nl}^{\mathrm{HO}}(r)$ with $N < 12$ are exactly forbidden states of the RGM. Therefore, in order for the above-mentioned link between the local potential model and the RGM to be sufficiently meaningful, the expansion coefficients C_{Nl} for $N < 12$ in Eq. (5.6) should be vanishingly small. If this condition for C_{Nl} is actually satisfied, we can put C_{Nl} for $N < 12$ to be exactly zero in calculating M_l by using Eq. (5.7). This point was investigated in Ref. 30 and it was found that C_{Nl} for $N < 12$ are actually very small. It is to be noticed if $u_l(r)$ is equal to $u_{12,l}^{\mathrm{HO}}(r)$ (namely $C_{Nl} = \delta_{N,12}$) Φ_l is exactly the same as the SU(3) shell model wave function $(pf)^4[4](12,0)$. In general, the coefficient $C_{12,l}$ of Eq. (5.6) is just the amplitude of the component $(pf)^4[4](12,0)$ contained in Φ_l. If C_{Nl} are large only for $N \approx 12$, Φ_l is close to the shell-model limit and expresses the state with strong overlap between clusters, while if Φ_l represents the well-developed clustering state, C_{Nl} spreads up to high N. Now we compare the expression of M_l' with that of M_l in Eq. (5.7). Since $m(N,N',l)$ is nonvanishing only for $|N - N'| \le 2$, it is clear that M_l' and M_l are close to each other if the ratios $(\mu_{N-2}/\mu_N)^{1/2}$ are close to unity. It is well known that for large N, $(\mu_{N-2}/\mu_N)^{1/2}$ is close to unity because $\mu_N \to 1$ for $N \to \infty$, and therefore M_l' and M_l are close to each other in the case of well-developed clustering states Φ_l. However, on the contrary, for $N \approx 12$, $(\mu_{N-2}/\mu_N)^{1/2}$ is appreciably smaller than unity, and therefore M_l' and M_l can differ largely from each other in the case of the states with strong overlap between clusters. In Table II we compare the $B(E2)$ values calculated by M_l' with those by M_l in the case of the potential model of Ref. 11 (and 30). Here the calculation of M_l' is done in two ways. First, like Ref. 11 (and 30), M_l' is calculated by not putting C_{Nl} for $N < 12$ to be zero. Second, we have calculated M_l' by putting C_{Nl} for $N < 12$ to be zero and the resulting values are denoted as M_l''. We see that the $B(E2)$ values by M_l' and M_l'' are larger than those by M_l by about 15% and 30%, respectively. The reason why $|M_l'|$ (or $|M_l''|$) is larger than $|M_l|$ for the states near the shell-model limit is easily understood by the following allowable simplification for $u_l(r)$:

TABLE II. Comparison of the $B(E2)$ values calculated by M_l' and M_l'' with those by M_l in the case of the potential model of Ref. 11 (and Ref. 30) and in the case of the RGM treatment of Ref. 13. As for the definition of M_l', M_l'', and M_l, see the text. The $B(E2)$ values calculated by M_l' in the same RGM framework as Ref. 13 are slightly different from those reported in Ref. 13. This may be due to the difference of the calculation of the Coulomb kernel which is done exactly in Ref. 13.

	$B(E2)$ $(J\to J-2)$ $(e^2\text{fm}^4)$				
	Ref. 11			Ref. 13	
J^π	M_l'	M_l''	M_l	M_l'	M_l
2^+	107.3	124.1	93.3	130.7	97.4
4^+	146.4	171.4	128.0	173.6	129.1
6^+	140.2	169.1	125.2	164.0	121.7
8^+	118.1	146.8	107.4	130.5	97.2
10^+	74.9	98.7	72.8	84.5	64.2
12^+	33.6	43.3	33.5	38.3	30.5

$$u_l(r)=\alpha u^{\text{HO}}_{12,l}(r)+\beta u^{\text{HO}}_{14,l}(r)\ , \tag{5.8}$$

which is obtained by neglecting the small components with $N\geq 16$ (and $N<12$) and by neglecting the small l dependence of the expansion coefficients for $N=12$ and 14. The sign of α is opposite to that of β, $\alpha\beta<0$. This is due to the general property of the expansion coefficient C_{Nl} which changes its sign for the change of N, $N\to N+2$. By Eq. (5.8), M_l' and M_l are expressed as

$$\begin{aligned} M_l' &= A_l+B_l\ , \\ M_l &= A_l+\left[\frac{\mu_{12}}{\mu_{14}}\right]^{1/2} B_l\ , \\ A_l &= \alpha^2 m(12,12,l)+\beta^2 m(14,14,l)\ , \\ B_l &= \alpha\beta[m(12,14,l)+m(14,12,l)]\ . \end{aligned} \tag{5.9}$$

It is easy to get the following formulas:

$$\begin{aligned} m(N,N,l) &= -\frac{[(N+l+1)(N-l+2)]^{1/2}}{2\gamma}\cdot k_l\ , \\ m(N,N+2,l) &= \frac{[(N+l+1)(N+l+3)]^{1/2}}{4\gamma}\cdot k_l\ , \\ m(N+2,N,l) &= \frac{[(N-l+2)(N-l+4)]^{1/2}}{4\gamma}\cdot k_l \\ k_l &= \frac{4\times 40}{44}\langle Y_{l-2,0}\,|\,Y_{20}\,|\,Y_{l0}\rangle\ . \end{aligned} \tag{5.10}$$

From Eq. (5.10) and the relation $\alpha\beta<0$, we see that A_l and B_l are of the same sign. Hence, the relation $\mu_{12}/\mu_{14}<1$ ($\mu_{12}=0.069$, $\mu_{14}=0.264$) (Ref. 41) leads to the relation $|M_l'|>|M_l|$.

Next we consider the calculation of the $B(E2)$ values of Ref. 13. In Ref. 13, the $B(E2)$ matrix elements are calculated by the RGM wave function $\mathcal{A}[\chi_l(r)Y_{l0}(\hat{r})\phi(\alpha)\phi(^{40}\text{Ca})]$ in an approximate way as follows:

$$\begin{aligned} M_l' &= \langle \chi_{l-2}(r)Y_{l-2,0}(\hat{r})\,|\,\hat{N}^{1/2}\bar{y}_{20}(\mathbf{r})\hat{N}^{1/2}\,|\,\chi_l(r)Y_{l0}(\hat{r})\rangle \\ &= \langle \omega_{l-2}(r)Y_{l-2,0}(\hat{r})\,|\,\bar{y}_{20}(\mathbf{r})\,|\,\omega_l(r)Y_{l0}(\hat{r})\rangle\ , \\ \omega_l(r)Y_{l0}(\hat{r}) &= \hat{N}^{1/2}\chi_l(r)Y_{l0}(\hat{r})\ . \end{aligned} \tag{5.11}$$

Thus the calculational procedure of the $B(E2)$ matrix element of Ref. 13 is the same as that of the local potential model given in Eq. (5.2). By denoting the coefficients of the expansion of $\omega_l(r)$ by $u^{\text{HO}}_{Nl}(r)$ also as C_{Nl}, we can express M_l' and the exact $B(E2)$ matrix element M_l by Eq. (5.7). The comparison of the $B(E2)$ values of Ref. 13 calculated by using M_l' with the exact $B(E2)$ values obtained by using M_l is also displayed in Table II. We see again that the former values are larger than the latter values by about 30%. In Ref. 13 it is mentioned that in the case of the ground rotational band of the $\alpha+^{16}$O system, $|M_l'|^2$ differs from $|M_l|^2$ within about 10–20%. The reason why the difference between $|M_l'|^2$ and $|M_l|^2$ in the $\alpha+^{16}$O system is smaller than that in the $\alpha+^{40}$Ca system is largely due to the fact that the ratio μ_8/μ_{10} ($\mu_8=0.229$, $\mu_{10}=0.510$) (Ref. 41) of the lowest two eigenvalues of the normal kernel of the $\alpha+^{16}$O system is closer to unity than the corresponding ratio μ_{12}/μ_{14} in the $\alpha+^{40}$Ca system.

As for the other spectroscopic problems relevant to the present analyses, we will discuss them in another part. One of such problems is the question which state is to be described by the calculated second 0^+ state, 8.54 MeV 0^+ state or 11.2 MeV 0^+ state. The related question is which group of observed states correspond to the calculated $K^\pi=0^+$ band starting with this calculated second 0^+ state. Here in this paper we would like to present one conclusion which can be derived from the analyses of Sec. III. That is, contrary to Refs. 15, 18, 19, and 21, it is unlikely that there appears a mixed-parity rotational band with its band head position around 6 MeV above the $\alpha+^{40}$Ca threshold.

Next, in the remaining part of this section, we discuss the equivalent local potential to the $\alpha+^{40}$Ca RGM nonlocal potential. For this purpose we utilize the l-averaged ELP $V^{\text{ELP}}(r)$ which is obtained by the use of the HNY force with $\Delta=50$ MeV and which has been shown in Sec. III to be almost identical in shape to the optical potential by Delbar *et al.*[7] In Fig. 8 we display the decomposition of $V^{\text{ELP}}(r)$ into the direct (or double folding) potential $V_D(r)$ and the exchange potential $\Delta V(r)$; $V^{\text{ELP}}(r)=V_D(r)+\Delta V(r)$. The energy dependence of $V^{\text{ELP}}(r)$ is due solely to that of $\Delta V(r)$, since $V_D(r)$ is independent of the incident energy. In this figure we also display $V^{\text{opt}}(r)$ of Ref. 7 to which $V^{\text{ELP}}(r)$ is seen to be very close.

What we learn first from this figure is the theoretical explanation of the reason why $V^{\text{opt}}(r)$ is deep. The reason is attributed to the smallness of the exchange potential $\Delta V(r)$ compared to the deep direct potential $V_D(r)$. It has often been mentioned that the exchange potential becomes larger (or more repulsive) as the internucleus distance becomes smaller, namely as the overlap of two nuclei becomes larger. This, however, is not true as has been extensively studied.[31–35] The reason is as fol-

lows. As two nuclei overlap more heavily, the exchange process of larger number of nucleons between nuclei becomes possible. Thus it looks like as if the exchange potential became larger. An important point here is the recognition that the exchange process of larger and larger number of nucleons yields a nonlocal interaction between nuclei with longer and longer range of nonlocality. The long nonlocality range means directly the short energy range. Namely, as the energy gets higher the wavelength of the wave function becomes shorter and the nonlocal potential with long nonlocality range becomes rapidly more ineffective when integrated with such short-wavelength wave function. Thus the larger the number of exchanged nucleons is, the shorter the range of the nonlocal potential coming from such exchange process is, not only spatially but also energetically. According to this general argument, an attractive internuclear potential $U(r)$ works so as to make the exchange potential due to many-nucleon-exchange process ineffective in the whole spatial region. The reason is as follows: Such exchange potential can be effective only in the spatial region of small internucleus distance, but since in such a re-

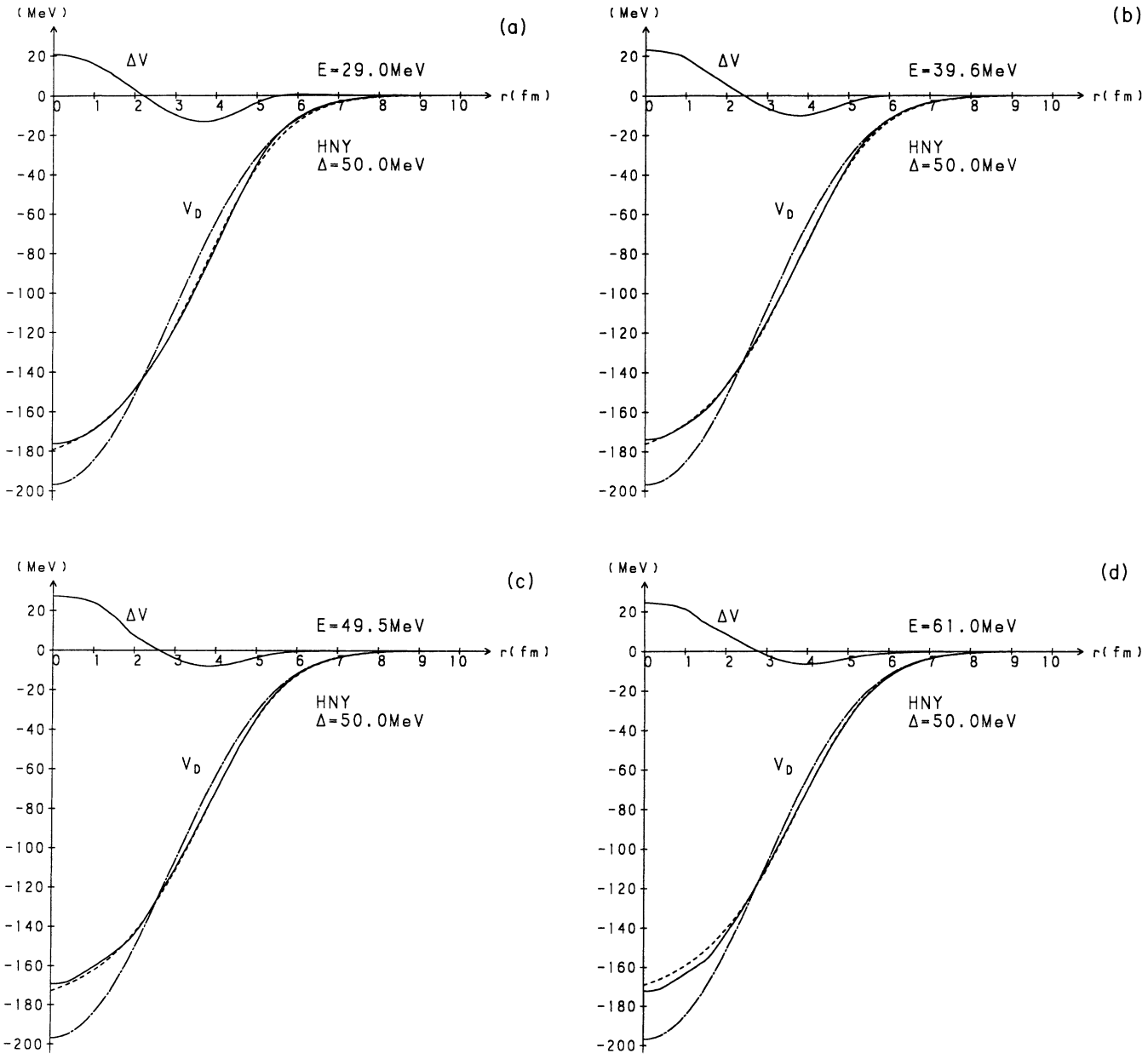

FIG. 8. Decomposition of the real part of the l-averaged equivalent local potential $\mathrm{Re}[V^{\mathrm{ELP}}(r)]$ (solid curve) into the direct potential $V_D(r)$ (dashed-dotted curve) and the exchange potential $\Delta V(r)$ (upper solid curve). (a), (b), (c), and (d) are for $E=29.0$, 39.6, 49.5, and 61.0 MeV, respectively. The HNY force with $\Delta=50$ MeV is used for the calculation of V^{ELP}. Here the real part of the optical potential of Delbar *et al.* $\mathrm{Re}[V^{\mathrm{opt}}(r)]$ is also displayed by the dashed curve.

gion the effective energy for the internucleus relative motion, $E_r+U(r)$, is high even for low incident energy E_r, the exchange potential is forced to be largely less effective. According to the actual numerical studies, in the case of light-ion projectiles such as α particle, the exchange potentials due to more-than-one-nucleon exchange are vanishingly small and hence the total exchange potential is almost exhausted by the one-nucleon exchange potential in the whole spatial region. Note here that even the one-nucleon exchange potential is reduced in its magnitude due to the same combined effect of its nonlocality and the attractive potential.

In Fig. 8 we see that the *mild* energy dependence of $V^{\rm opt}(r)$ to become shallower as E gets higher is very nicely reproduced by the energy dependence of $\Delta V(r)$. The mildness of the energy dependence of $V^{\rm opt}(r)$ is explained to be largely due to the small magnitude of $\Delta V(r)$. The tendency of $V^{\rm opt}(r)$ to become shallower for higher E is explained to be mainly due to the following three characteristics of $\Delta V(r)$.[31–35] The first is the attractive nature of $\Delta V(r)$ in the tail region. It has been often argued that the exchange internucleus potential is repulsive since the exchange potential originates from the Pauli exclusion process. This, however, is not necessarily true. A good example is the exchange potential of the single nucleon potential. It is the so-called Fock potential and as is well known to be largely attractive. The second characteristic is that this attractive part of $\Delta V(r)$ becomes smaller in its magnitude as E gets higher. It is due to the general fact that the exchange effect becomes smaller for higher E. The third characteristic of $\Delta V(r)$ is that the repulsive part of $\Delta V(r)$ in the region of the short relative distance becomes more repulsive as E gets higher. This repulsive part of $\Delta V(r)$ consists mainly of the repulsive contribution coming from the short range repulsion of the adopted effective two-nucleon force. In general, as E gets higher, the exchange potential coming from the shorter range part of the effective two-nucleon force becomes smaller more slowly than that from the longer range part does. Hence the faster diminishing nature of the attractive component of $\Delta V(r)$ than that of the above-mentioned repulsive component of $\Delta V(r)$ makes the net repulsive part of $\Delta V(r)$ become more repulsive for higher E.

The magnitude of the energy dependence of $V^{\rm ELP}$ is largely governed by the adopted effective two-nucleon force. If we use an affective two-nucleon force which yields similar bound and quasibound state spectra to the present effective force (the HNY force with $\Delta=50$ MeV), but which has a larger Majorana component than the present force, the direct potential becomes shallower than the present one shown in Fig. 8, but the exchange potential becomes deeper than the present one shown also in Fig. 8. The net depth of the $V^{\rm ELP}$, however, remains almost unchanged for the low scattering energy, the reason of which is discussed in detail in Ref. 42. When the exchange potential is larger, the energy dependence becomes necessarily large. Thus the fitting of the scattering data in a wide energy range necessarily imposes rather strict condition for the character of the effective two-nucleon force to be selected.

As for the origin of the energy dependence of $V^{\rm opt}$, in general, we need to consider other effects than the internucleus antisymmetrization effect which is fully treated in the RGM. Among such other effects are included the renormalization effects on the elastic channel of the nonelastic processes which have been extensively studied recently.[43] However, in the energy range, $E\approx 30-60$ MeV, treated in this paper, we are not faced with any significant need to take into account such other effects. On the other hand, when the energy E gets higher than about 60 MeV, as is seen in Fig. 6 where the energy dependence of the volume integral j_V of the real part of $V^{\rm opt}$ (Re$[V^{\rm opt}]$) is compared with j_V of Re$[V^{\rm ELP}]$, we find that j_V of Re$[V^{\rm opt}]$ seems to decrease more rapidly than j_v of Re$[V^{\rm ELP}]$. Thus in the high energy region, about 60 MeV, where the internucleus antisymmetrization effect is responsible for a significant part of the energy dependence of Re$[V^{\rm opt}]$, there seems to exist other effects which also contribute significantly to the energy dependence of Re$[V^{\rm opt}]$.

VI. CONCLUSION

The $\alpha+^{40}$Ca elastic scattering data at $E=29.0$, 39.6, 49.5, and 61.0 MeV are found to be reproduced very well by the $\alpha+^{40}$Ca RGM with the introduction of a phenomenological imaginary potential if one uses the suitably chosen effective two-nucleon forces. The adopted imaginary potential is the same as that of the $\alpha+^{40}$Ca optical potential of Delbar *et al.*[7] which is known to fit the scattering data very well in a wide energy range.

The angular-momentum-averaged ELP constructed from the RGM nonlocal potential is found to be very close to the optical potential of Delbar *et al.*

In our previous study[1] of the $\alpha+^{16}$O system we have already found similar results as above that the $\alpha+^{16}$O elastic scattering data in the energy range 20 MeV $\lesssim E \lesssim$ 70 MeV are reproduced very well by the $\alpha+^{16}$O RGM, by the use of a phenomenological imaginary potential, and that the angular-momentum-averaged ELP is very close to the $\alpha+^{16}$O optical potential of Michel *et al.*[2] which fits the scattering data very well in a wide energy range.

It is now believed that the discrete ambiguity of the optical potentials for light-ion projectiles such as ^{3}He and α can be removed by use of the high energy scattering data exhibiting the nuclear rainbow effect.[3] Therefore, any microscopic theory of the internucleus potential is now required to reproduce at least the essential features of these light-ion unique optical potentials. The real part of the unique optical potential is always very deep. We remember well that the anomalous large-angle scattering (ALAS) phenomena of α particle was nicely resolved by the introduction of the deep folding-type and weakly absorptive optical potential by Michel and Vanderpoorten[44] by rejecting various other explanations such as the parity dependence of the optical potential.[45] This has allowed an excellent theoretical explanation of the ALAS phenomena by Brink and Takigawa.[46] The present authors and their collaborators have been studying the internucleus potentials microscopically by deriving them by the

RGM and have already shown that the basic properties of the derived potentials are in good agreement semiquantitatively with those of the real parts of the unique light-ion optical potentials.[33–35] The $\alpha+^{40}$Ca optical potential of Delbar *et al.* and the $\alpha+^{16}$O optical potential of Michel *et al.* are well known as the unique optical potentials. Therefore, the above-mentioned results of the present study of the $\alpha+^{40}$Ca elastic scattering together with the similar results of the previous study[1] of the $\alpha+^{16}$O system fortifies our opinion that the RGM is powerful and quantitatively reliable for the microscopic study of the internucleus interaction including the microscopic foundation of the internucleus optical potential.

According to the extrapolation of the volume integral value of the real part of the ELP over $E\approx 60$ MeV, it seems that the energy dependence of the real part of the present ELP which comes only from the internucleus antisymmetrization effect is weaker than that of the real part of the optical potential over $E\approx 60$ MeV. This means that in addition to the internucleus antisymmetrization effect, there seem to exist other effects[43] which also contribute significantly to the energy dependence of the real part of the optical potential. The expected other effects should be repulsive effects that increase as E increases. The similar conclusion was also obtained in the $\alpha+^{16}$O system for $E\gtrsim 60$ MeV in Ref. 1.

When one calculates the bound and quasibound level spectra by the $\alpha+^{40}$Ca RGM which fits the elastic scattering data well, the calculated lowest 0^+ state is obtained below $\alpha+^{40}$Ca threshold and the calculated second 0^+ state is located around 6.5 MeV above the threshold. On the other hand, if one uses such effective two-nucleon force that locates the calculated lowest 0^+ state at the position of the observed 8.54 MeV 0^+ state (3.4 MeV above the threshold) or the observed 11.2 MeV 0^+ state (6.1 MeV above the threshold) since except the ground state these states are the lowest 0^+ states which have large α strength, the fitting of the calculated cross sections to the experimental ones is very bad. These two results force us to regard that the ground band structure of ^{44}Ti contains a large amount of the $\alpha+^{40}$Ca clustering component. This conclusion is consistent with that of the recent study of the $\alpha+^{40}$Ca fusion cross section by the optical potential model of Refs. 10 and 11.

The most serious objection to this conclusion is the fact that the RGM calculation which locates its lowest 0^+ level near the ^{44}Ti ground state cannot avoid the appearance of the negative parity rotational band with its bandhead 1^- state below the excitation energy 10 MeV although there have been reported no such experimental indications at all. Our present RGM study predicts the location of the band head 1^- state in the approximate energy region from 0 to 5 MeV above the $\alpha+^{40}$Ca threshold which therefore should be actively searched for experimentally. Thus our standpoint is essentially the same as that of Refs. 10 and 11 whose authors insist that there should exist a negative parity rotational band starting just above the threshold.

[1] T. Wada and H. Horiuchi, Phys. Rev. Lett. **58**, 2190 (1987).
[2] F. Michel, J. Albinski, P. Belery, Th. Delbar, Gh. Grégoire, B. Tasiaux, and G. Reidemeister, Phys. Rev. C **28**, 1904 (1983).
[3] D. A. Goldberg and S. M. Smith, Phys. Rev. Lett. **29**, 500 (1972); D. A. Goldberg, S. M. Smith, and G. F. Burdzik, Phys. Rev. C **10**, 1362 (1974).
[4] Y. Fujiwara, H. Horiuchi, K. Ikeda, M. Kamimura, K. Kato, Y. Suzuki, and E. Uegaki, Prog. Theor. Phys. Suppl. No. **68**, 29 (1980); T. Tomoda and A. Arima, Nucl. Phys. **A303**, 217 (1978).
[5] Y. Yamamoto, Prog. Theor. Phys. **52**, 471 (1974); A. Hasegawa and S. Nagata, *ibid.* **45**, 1786 (1971).
[6] T. Matsuse, M. Kamimura, and Y. Fukushima, Prog. Theor. Phys. **53**, 706 (1975).
[7] Th. Delbar, Gh. Grégoire, G. Paic, R. Ceuleneer, F. Michel, R. Vanderpoorten, A. Budzanowski, H. Dabrowski, L. Freindl, K. Grotowski, S. Micek, R. Planeta, A. Strzalkowski, and K. A. Eberhard, Phys. Rev. C **18**, 1237 (1978).
[8] H. Horichi, Prog. Theor. Phys. **73**, 1172 (1985).
[9] U. Strohbusch, C. L. Fink, B. Zeidman, H. W. Fulbright, R. G. Markham, and R. N. Horoshko, Phys. Rev. C **9**, 965 (1974).
[10] F. Michel, G. Reidemeister, and S. Ohkubo, Phys. Rev. C **34**, 1247 (1986).
[11] F. Michel, G. Reidemeister, and S. Ohkubo, Phys. Rev. Lett. **57**, 1215 (1986).
[12] A. B. Volkov, Nucl. Phys. **74**, 33 (1965).
[13] H. Kihara, M. Kamimura, and A. Tohsaki-Suzuki, in *Proceedings of the International Conference on Nuclear Structure, Contributed Papers,* edited by the Organizing Committee (International Academic Printing Co. Ltd., Tokyo, 1977), pp. 234 and 235.
[14] D. Frekers, H. Eikhoff, H. Löhner, K. Poppensieker, R. Santo, and C. Wiezorek, Z. Phys. A **276**, 317 (1976).
[15] D. Frekers, R. Santo, and K. Langanke, Nucl. Phys. **A394**, 189 (1983).
[16] A. Arima, in *Proceedings of the Topical Conference on Physics of Medium Light Nuclei,* edited by P. Blasi and R. A. Ricci (Editrice Compositori, Bologna, 1978), p. 19.
[17] K. Itonaga, Prog. Theor. Phys. **66**, 2103 (1981).
[18] K. Friedrich and K. Langanke, Nucl. Phys. **A252**, 47 (1975).
[19] K. Langanke, Nucl. Phys. **A377**, 53 (1982).
[20] D. M. Brink and E. Boeker, Nucl. Phys. **A91**, 1 (1967).
[21] H. Fredrich, K. Langanke, A. Weiguny, and R. Santo, Phys. Lett. **55B**, 345 (1975).
[22] K. Wildermuth and Y. C. Tang, *A Unified Theory of the Nucleus* (Vieweg, Braunschweig, 1977).
[23] H. Horiuchi, Suppl. Prog. Theor. Phys. **62**, 90 (1977).
[24] H. Horiuchi, Prog. Theor. Phys. **64**, 184 (1980).
[25] F. Michel and R. Vanderpoorten, Phys. Lett. **82B**, 183 (1979).
[26] H. P. Gubler, V. Kiebele, H. O. Meyer, G. R. Plattner, and I. Sick, Nucl. Phys. **A351**, 29 (1981).
[27] K. Aoki and H. Horiuchi, Prog. Theor. Phys. **67**, 1236 (1982).
[28] T. Wada and H. Horiuchi, Prog. Theor. Phys. **80**, 488 (1988); **80**, 502 (1988).
[29] K. Hatogai, M. Ohta and S. Okai, Prog. Theor. Phys. **68**, 2014 (1982).
[30] F. Michel, G. Reidemeister, and S. Ohkubo, Phys. Rev. C **37**, 292 (1988).
[31] K. Aoki and H. Horiuchi, Prog. Theor. Phys. **66**, 1508 (1981).
[32] K. Aoki and H. Horiuchi, Prog. Theor. Phys. **68**, 1658 (1982);

68, 2028 (1982).
[33]H. Horiuchi, K. Aoki, and T. Wada, in *Proceedings of the 1983 RCNP International Symposium on Light Ion Reaction Mechanisms,* edited by H. Ogata, T. Kammuri, and I. Katayama, 1983, p. 806 (unpublished).
[34]H. Horiuchi, in *Proceedings of the International Conference on Clustering Aspects of Nuclear Structure and Nuclear Reactions,* edited by J. S. Lilley and M. A. Nagarajan (Reidel, Dordrecht, 1985), p. 35.
[35]T. Wada and H. Horiuchi, J. Phys. Soc. Jpn. **54**, Suppl. II, 53 (1985).
[36]A. Arima, H. Horiuchi, K. Kubodera, and N. Takigawa, in *Advances in Nuclear Physics,* edited by M. Baranger and E. Vogt (Plenum, New York, 1972), Vol. 5, Chap. 3, p. 345.
[37]R. C. Barret and D. F. Jackson, *Nuclear Sizes and Structure* (Claredon, Oxford, 1977).
[38]B. Buck, H. Friedrich, and C. Wheatley, Nucl. Phys. **A275**, 246 (1977).
[39]S. Saito, Suppl. Prog. Theor. Phys. **62**, 11 (1977).
[40]H. Horiuchi, Prog. Theor. Phys. **71**, 535 (1984).
[41]H. Horiuchi and Y. Suzuki, Prog. Theor. Phys. **49**, 1974 (1973).
[42]H. Horiuchi, Prog. Theor. Phys. **69**, 886 (1983).
[43]M. A. Nagarajan, C. Mahaux, and G. R. Satchler, Phys. Rev. Lett. **54**, 1136 (1985); C. Mahaux, H. Ngo, and G. R. Satchler, Nucl. Phys. **A449**, 354 (1986); **A456**, 135 (1986).
[44]F. Michel and A. Vanderpoorten, Phys. Rev. C **16**, 142 (1977).
[45]For example, Y. Kondo, S. Nagata, S. Ohkubo, and O. Tanimura, Prog. Theor. Phys. **53**, 1006 (1975).
[46]D. M. Brink and N. Takigawa, Nucl. Phys. **A279**, 159 (1977).
[47]G. Gaul, H. Lüdecke, R. Santo, H. Schmeing, and R. Stock, Nucl. Phys. **A137**, 177 (1969).
[48]H. Eickhoff, D. Frekers, H. Löhner, K. Poppensieker, R. Santo, G. Gaul, C. Mayer-Böricke, and P. Turek, Nucl. Phys. **A252**, 333 (1975).
[49]D. A. Goldberg, Phys. Lett. **55B**, 59 (1975).
[50]I. Brissaud and M. K. Brussel, J. Phys. C **3**, 481 (1977).
[51]J. J. Simpson, W. Dünnweber, J. P. Wurm, P. W. Green, J. A. Kuehner, W. R. Dixon, and R. S. Storey, Phys. Rev. C **12**, 468 (1975); J. Britz, A. Chevallier, J. Chevallier, and B. Haas, Nucl. Phys. **A262**, 189 (1976).